Boosted energy-storage efficiency by controlling conduction loss of multilayered polymeric capacitors

Francesco Pedroli, Annalisa Flocchini, Alessio Marrani, Minh-Quyen Le, Olivier Sanseau, Pierre-Jean Cottinet, Jean-Fabien Capsal

Boosted energy-storage efficiency by controlling conduction loss of multilayered polymeric capacitors

Francesco PEDROLI[a/b], Annalisa FLOCCHINI[a], Alessio MARRANI[c], Minh-Quyen LE[a], Olivier SANSEAU[b], Pierre-Jean COTTINET[a], Jean-Fabien CAPSAL[a]

[a]Univ Lyon, INSA-Lyon, LGEF, EA682, F-69621, Villeurbanne, France; [b]P2D, CNRS/Rhodia-Solvay, UMR 5268, 85 avenue des Frères Perret, F-69192 Saint Fons, France; [c]Solvay Specialty Polymers, viale Lombardia 20, 20021 Bollate, Italy

[†]corresponding author: jean-fabien.capsal@insa-lyon.fr

Abstract

Among the organic dielectrics, polyvinylidene fluoride PVDF-based polymers present the highest level of polarizability with permittivity greater than 35. Nonetheless, their applications in advanced electronics and industrial uses are limited by significant leakage current under high voltage, which is considered the principal cause of device energy consumption and short lifetime. Therefore, the main objective of this paper was to focus on alternative capacitor structure-based polyvinylidene fluoride-trifluoroethylene-chlorotrifluoroethylene (PVDF-TrFE-CTFE) terpolymers to efficiently limit the leakage current and lead to enhanced electrical breakdown with negligible degradation of polarization level. The novel bilayer capacitor was constructed by depositing a thin barrier layer of high polar PVDF-HFP copolymer on the terpolymer via a rapid solution-casting technique. The relationship between leakage current, dielectric strength and conduction mechanisms was investigated. Implementation of such a barrier layer led to a significant reduction (70%) in leakage current and ferroelectric losses (approximately 90%), thus boosting the performance of multilayered material up to 50% of enhanced energy-storage efficiency. Experimental results are very promising, allowing to confirm that combining both terpolymer and copolymer in a hybrid multilayer design makes a possibility to achieve the best compromise in terms of energy efficiency, dielectric properties, and breakdown strength.

Keywords

Multi-layered film capacitor, electrical breakdown, energy-storage, leakage current, conduction loss

1. Introduction

Electrostatic capacitors are key components in advanced electronic devices and pulse-power systems due to their large energy density levels (in the order of tens of Joule per cube centimeter) [1,2] and readiness to deliver stored energy (today, pulse-widths of hundreds of microseconds are achieved even at megavolt levels) [3]. On the other hand, in the race to achieve electronic device miniaturization, many challenges have to be overcome to achieve capacitor size reduction, which still needs to occupy more than 50% of the whole volume device in order to guarantee the required power supply to the application. In this sense, dielectric polymers possess successful features, such as easy processability, light weight, flexibility, self-healing, low dissipation factor, and large electrical breakdown [4–11]. Nevertheless, this class of materials still suffers from relatively low dielectric constants (≈3 for the commercialized polymeric capacitors, such as biaxially oriented polypropylene [BOPP] or polycarbonate [PC] capacitors) [12] and consequently have limited dielectric polarization with respect to conventional ceramic dielectrics. Among the dielectric polymers, the polyvinylidene fluoride (PVDF)-based polymers exhibit excellent polarizability due to spontaneous polarization of the highly polar molecular C–F bonds [13,14]. An exceptional capacitor is one consisting of the relaxor-ferroelectric polyvinylidene fluoride-trifluoroethylene-chlorotrifluoroethylene/chlorofluoroethylene (PVDF-TrFE-CTFE/CFE) terploymer. This type of polymer presents the

possibility to exploit additional polarization mechanisms [15,16] (such as molecular dipole polarization) and shows dielectric permittivity even larger than 30 at relatively high frequency of 1kHz [17,18]. However, the main drawback of the PVDF-based polymers stems from high conduction losses principally caused by significant leakage currents. This drawback seriously limits their wide industrial use in next-generation power systems.

With the aim of efficiently enhancing the performance of ferroelectric and relaxor-ferroelectric polymers, the most common approach (based on the scientific community's point of view) consists of increasing the dielectric constant so as to achieve satisfactory polarization level at a lower applied electric field. In most cases, this technique involves the realization of polymer nano/micro-composites by doping of high-*k* or conductive inorganic fillers [19–22] with very large values of dielectric permittivity (> 10^3) [23–27]. However, in general, the great potential of these systems is not accessible because the introduction of fillers gives rise to higher leakage current, leading to a dramatic decline in polymer dielectric strength [28], charge-discharge efficiency and capacitor life-time [29–31] Leakage currents are of fundamental relevance for achieving high-performing and long-life polymer devices since ohmic losses are the main cause of power dissipation [32] and self-heating [33], thus leading to early material degradation [34–37] The other relevant consideration for energy storage devices is the charge–discharge efficiency. Low charge-discharge efficiency is the result of large energy losses that will contribute to heat generation (Joule effect) [38,39].

An alternative approach for decreasing the leakage current consists of blending the highly polar PVDF co- and terpolymers with more insulating polymers, such as polyamides [40], polyurethanes [41], polyethylene [42], polythiourea [43], polypropylenes [44,45], polystyrene [46], and polyacrylates [47]. Among the reported materials, blends of poly-methyl methacrylate (PMMA) have proved to be the most effective due to the high affinity with fluorinated polymers [48,49]. Nevertheless, to achieve significant improvements in charge–discharge efficiency, large concentrations of PMMA are required (> 30%$_w$) [50–52], leading to a fall in material polarizability as well as energy-storage density. In order to overcome this drawback, another advanced technique has been recently investigated by Baer and Zhu through the realization of multilayered structures based on alternating films of PVDF-hexafluoropropylene (HFP) and PC [53,54] or PVDF and polysulfone (PSF) [55,56]. Based on the same approach, in the later years multilayered polymeric capacitor structures have been widely investigated and noteworthy advances in terms of increased energy-storage efficiency are reported [39,56–65]. Contrary to blends and composites, multilayered structures possess additional advantages due to their barrier interfaces perpendicular to the direction of applied electric field and therefore, to the traveling direction of electric charges forming the conduction loss [66]. In addition to charge barrier effects, the presence of perpendicular interfaces formed by materials having different electrical conductivity yields space-charged regions [55,67], which hinder electron conduction and homo-charge injection from the electrodes [32,68–70].

In this work, we propose an effective solution for successfully enhancing the energy-storage properties of the highly polarizable relaxor-ferroelectric PVDF-TrFE-CTFE terpolymer with an exceptional dielectric permittivity of ε_r = 60. This method involves a bilayer architecture consisting of a PVDF-TrFE-CTFE terpolymer and PVDF-HFP copolymer elaborated via solution-casting, which is a simple technique for polymer multilayer stacking. In contrast to the former multilayered structures reported by Baer and Zhu [53–56] whose barrier material is made of an insulating polymer with very limited dielectric constant (such as $\varepsilon_r \approx 2$), in this study, the selected barrier layer PVDF-HFP copolymer possessed a much larger dielectric constant ($\varepsilon_r \approx 12$). Moreover, its thickness was chosen to be very small (in the order of tens of microns) with respect to the whole sample thickness so as not to degrade the high polarization properties of the PVDF-TrFE-CTFE terpolymer layer. Finally, the proposed design allows for effective exploitation of the benefit of both terpolymer and copolymer materials. This design permitted creation of a simple way to decrease the leakage current through the dielectric polymer during high voltage application combined with enhancement of dielectric strength in addition to energy-storage efficiency of the whole polymer capacitor.

2. Materials and process

2.1. Single-layer film fabrication

The two kinds of polymers used in this work are the highly polar PVDF-TrFE-CTFE terpolymer and the insulating PVDF-HFP copolymer (called HFP, for the sake of simplicity) that have been provided by Solvay Specialty Polymers Italy S.p.a as a powder [71]. Selection of the terpolymer grade, including monomeric composition and molecular weight in addition to the manufacturing optimization in terms of solvent choice, material purification, and crystallization steps were described in our previous studies [18,32]. Barium titanate (purchased from US Research Nanomaterials Inc, Houston, TX), which is an inorganic compound with chemical formula BaTiO3 (or BTO) was selected as the nanoparticle material with an average size of 500 nm due to its commercially available use, effective cost, and high piezoelectric properties. For material characterizations, polymeric films are prepared by casting dissolutions of terpolymer, copolymer, and $BaTiO_3$-composites of copolymer. Pure polymeric dissolutions are prepared dissolving 25%$_{wt}$ and 10%$_{wt}$ of terpolymer and copolymer powder, respectively, in 2-butanone (also known as methyl ethyl ketone or MEK).

To obtain homogenous composite consisting of the PVDF-HFP copolymer filled with 10%$_{vol}$ or 20%$_{vol}$ $BaTiO_3$ nanoparticles, the whole solutions were mechanically agitated for approximately 12 h. Afterwards, dispersion of $BaTiO_3$ nanoparticles was achieved via a specific protocol based on ultrasound stirring as described in the next paragraph. It is noteworthy that PVDF-HFP/MEK solutions form polymer/solvent network-like structures (or gels) that exhibit extremely high viscosity; thus, they impede homogeneous dispersion of the nanoparticles. As a result, polymer concentration, operating temperatures, and filler content [72] play an important role in the formation of PVDF-HFP/MEK gels. Consequently, an optimized ultrasound treatment, including temperature control and duration, was developed in order to achieve the best compromise between lack of gel formation and solvent evaporation.

A flacon of composite solution was entirely immersed in a water bath at ambient temperature and agitated by two sonication periods (400W, Hielscher UP400St) lasting 2 min separated by a 1-min break. Finally, the as-prepared dissolutions were cast by mean of a calibrated doctor-blade on tempered glass plate. The PVDF-HFP composite films elaborated with 10%$_{vol}$ or 20%$_{vol}$ of $BaTiO_3$ (renamed HFP10BTO and HFP20BTO, respectively) in addition to films of pure PVDF-HFP copolymer have 10 mm x 250 mm rectangular shape with a thickness of 15 µm, which was perfectly controlled using a well-calibrated casting knife. Drying and annealing step were subsequently performed in a convection oven (Mermmet ULP400) under the temperature profile shown in Figure 1. The optimal annealing temperature was chosen as the start of the PVDF-TrFE-CTFE terpolymer melting peak [73] determined during the second melting differential scan calorimetry (DSC) ramp.

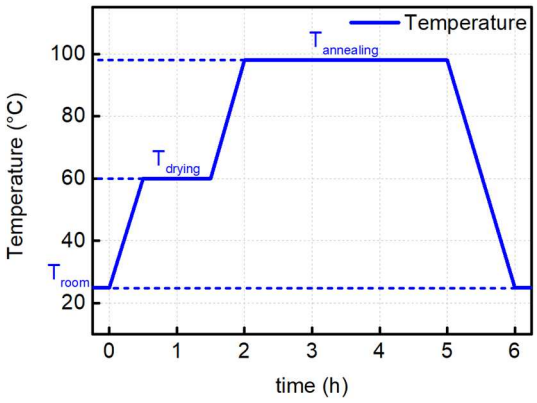

Figure 1. Drying and annealing profile temperature for polymer film manufacturing

2.2. Multilayered film fabrication

The design of a multilayered capacitor (Figure 2) consisted of a 65 µm-thick layer of a highly polar PVDF-TrFE-CTFE terpolymer layer stacked with an insulating layer acting as a barrier to conduction charges. The choice of the barrier materials consisted of the pure PVDF-HFP copolymer and its composites consisting of $BaTiO_3$ nanoparticles. The fabrication of the bilayer capacitor involved two steps: (1) film casting of terpolymer dissolution on the glass plate and its subsequent thermal treatments and (2) implementation of the barrier layer performed directly on top of the post-annealed terpolymer. After drying at ambient temperature, the multilayered sample was annealed for 1 h under controlled temperature of 98°C, which corresponds to the optimal terpolymer crystallization temperature. Finally, the bilayer structure was sandwiched between two 25nm-thick gold sputtering electrodes via a Cressington Sputter Coater (208 HR) in order to facilitate electrical contact.

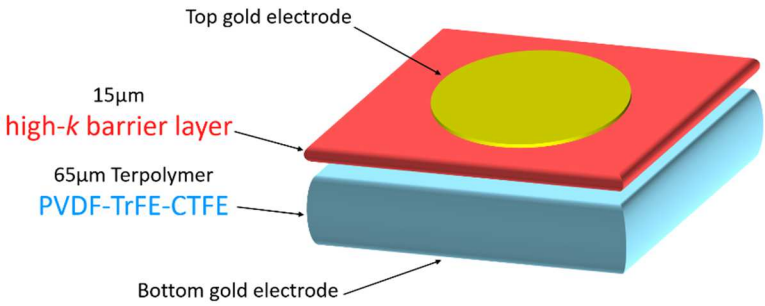

Figure 2. Multilayered capacitor structure.

3. Characterization methods

3.1. Thermal analysis

DSC measurements were performed on terpolymer and copolymer powders in order to determine the thermal characteristics, such as temperatures of onset and position of melting peak, of the two polymers. Thermographs were recorded during the second melting DSC ramp with a heating speed of 10 K/min.

3.2. Morphological characterization

The quality of the $BaTiO_3$ nanoparticle dispersion in the PVDF-HFP copolymer matrix in addition to the interface between the two-cast-layer PVDF-TrFE-CTFE/PVDF-HFP was checked via scanning electron microscopy (SEM). Samples were prepared via cryo-fracturing in liquid nitrogen in order to properly make the cross-section accessible. The morphologies of cross-section, later gold sputtered particles were imaged using the SEM FEG Ultra 55 by Zeiss with an accelerating voltage of 10 kV.

3.3. Electrical characterization

To perform electrical measurements, circular gold electrodes with 8mm-diameter and 25nm-thick were deposited on both sides of polymeric films in order to obtain capacitor-like architectures. Dielectric permittivity and dielectric losses were measured via broadband dielectric spectroscopy (BDS) by means of a Solartron 1260 impedance analyzer. Ambient temperature dielectric spectra were acquired under an AC $1V_{peak-peak}$ electrical voltage at frequency range of 10^{-1}–10^{6} Hz.

Dielectric strength of the fabricated materials was determined by application of an increasing DC ramp voltage at rate of 500 V/sec. Each polymeric film was subject to several electrical failure events in order to draw its breakdown probability distribution, which was determined according to the Weibull model:

$$P(E) = 1 - exp\left[-\left(\frac{E}{\lambda}\right)^{k}\right] \quad (1)$$

in which *P(E)* is the sample breakdown probability for a given electric field *E*, λ is the scaling parameter corresponding to breakdown strength at which 63.2% of the breakdowns occur, and *k* is the shape factor representing the spread of breakdown distribution. For each sample, the experimental breakdown probability distribution was fitted with the above Weibull equation by varying these two parameters λ and *k* so as to achieve the best consistence between measured data and theoretical estimation. According to the model, the "breakdown strength constant" of the sample is assumed to be equal to λ, that corresponded to a breakdown probability of 63% [74]. Eventually, experimental and model results illustrated on linear-scale graphs allowed to highlight the cumulative features of the failure probability distribution as described by the Weibull approach. Indeed, the exponential behavior exhibited quasi-linear trend under low applied electric fields that did not excess to the "breakdown strength constant" (i.e. equal to λ). Above this value, the failure probability quickly attained to a saturate regime, which corresponded to a plateau of 100% breakdown probability, especially under very high voltages.

The electrical resistivity of a polymeric capacitor can be deduced from a measurement of the experimental current under a unipolar DC electric field. This method allowed us to assume that the leakage current was principally caused by electron conduction. After a transient state in which all of the interfacial phenomena, including conduction of saturated ionic species [32], the intensity current then leveled off at a constant value, which represented the electron flow traversing the capacitor [75]. Hence, the DC electronic volume resistivity (ρ_{DC}) could be estimated according to the Ohm's law:

$$\rho_{DC} = \frac{E}{j_{leakage}^{DC}} \quad (2)$$

Here, *E* represents the applied DC electric field, and $j_{leakage}^{DC}$ is the current density detected after 6 h of unipolar DC electric field appliance.

Finally, in order to evaluate the polarization states and the dielectric responses of the selected materials under high voltage application, charge–discharge cycles were applied. Bipolar sinusoidal AC electric fields with a frequency of 100 mHz and amplitude of 50 V/µm were applied, and the experimental current was recorded by means of SIRIUS® cards (by Dewesoft). The electric displacement of the sample was then calculated as the integral of the current density. It was possible to consider the measured current density j_{tot} as the summation of a conduction current $j_{leakage}^{AC}$ and a capacitive current j_{cap} components:

$$j_{tot} = j_{leakage}^{AC} + j_{cap} \quad (3)$$

Within the electric field range used for the characterization, the fabricated materials possess a linear resistive behavior such that the resistive current component ($j_{leakage}^{AC}$) can be simply defined following Ohm's law. This method allowed for discrimination of a purely polarization current component j_{cap} from leakage currents $j_{leakage}^{AC}$ and thus calculations of electric displacements due to only material polarization process could be performed using Equation (4):

$$D(E) = \int j_{cap}\, dt \quad (4)$$

High voltage permittivity was defined as the electric field-derivative of the electric displacement:

$$\mathcal{E}(E) = \frac{dD(E)}{dE} \quad (5)$$

The evolution of dielectric permittivity at high voltages was also modeled by the two-component Debye/Langevin formalism [76] as expressed in Equation (6). Fitting the experimental polarization loops allows for the possibility of determining material parameters [18,77] relative to each phase of material and is one of the advantages of this method. Whenever the material is composed of amorphous and semi-crystalline phases as in the case of a semicrystalline terpolymer or of a polymer matrix and inorganic particles, such as for $BaTiO_3$-composites of PVDF-HFP, it is possible to use this formula. The material phase

parameters, such as dielectric permittivity at zero electric field ($\mathcal{E}_r(0)$) and saturation electric field (E_{sat}) allowed us to predict the dielectric response of pure polymers or polymer composites for a given applied electric field:

$$\mathcal{E}_r^{\theta}(E) = 3\,\mathcal{E}_r(0)\left[\left(\frac{E_{sat}^{\theta}}{E}\right)^2 - \left(sinh\frac{E}{E_{sat}^{\theta}}\right)^{-2}\right] \quad (6)$$

in which θ denotes the material phase. In case of a pure terpolymer matrix, θ signifies amorphous or crystal parts. Concerning a dielectric composite, such as PVDF-HFP/$BaTiO_3$, θ indicates copolymer matrix or $BaTiO_3$ nanoparticles.

The experimental polarization loop was then fitted by integrating the modeled capacitive current as defined by the equations (7) and (8). More detailed applications of Debye/Langevin formalism were described in our previous papers [18,32].

$$j_{cap}^{\theta} = \frac{dE}{dt}\,\mathcal{E}_0\,\mathcal{E}_r^{\theta}(E) \quad (7)$$

$$j_{cap} = \sum\nolimits_{\theta} j_{cap}^{\theta} \quad (8)$$

All data treatments were then performed using Origin software.

3.4. Energy-storage efficiency

Energy-storage efficiency (η) was derived via energy balance during charge–discharge loops (or electric displacement loops) and was defined as the ratio between the recoverable electrical energy ($U_{recovered}$) and the whole stored energy (U_{stored}) by the capacitor [78], which consisted of both recovered and lost energies $U_{recovered}$ and U_{loss}, respectively; see equation (9). In turn, lost energy (U_{loss}) included the dissipated energy due to conduction losses ($U_{leakage}$) and polymer hysteresis loss during discharge ($U_{hysteresis}$) as shown in equation (10).

$$\eta = \frac{U_{recovered}}{U_{stored}} = \frac{U_{recovered}}{U_{recovered} + U_{loss}} \quad (9)$$

$$U_{loss} = U_{leakage} + U_{hysteresis} \quad (10)$$

Electrical energy density was defined by the equation:

$$U_i = \int_0^{D_{max}} E\,dD(E) \quad (11)$$

Accordingly, the estimation of the recoverable electrical energy density ($U_{recovered}$) could be easily obtained by the integration of the area enclosed between the vertical axis and discharging curve of the electric displacement versus applied electric field loops [79] as represented in Figure 3 by the green shaded area while the stored energy density (U_{stored}) corresponded to the area delineated by the vertical axis and charging curve. Consequently, the lost energy (U_{loss}) was represented by the internal area of the electric displacement loop, corresponding to the red shaded area in Figure 3.

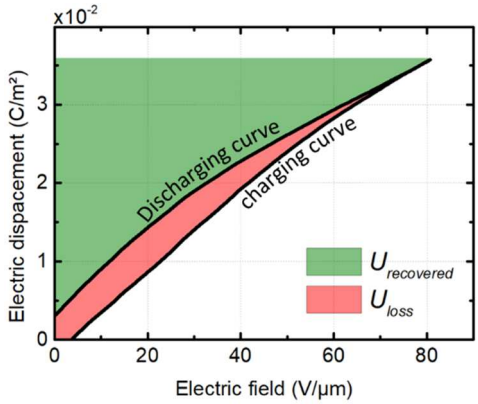

Figure 3. Generic charge–discharge loop for a dielectric material showing hysteresis. Green area depicts the recovered electric energy; red area represents the energy losses.

4. Results and discussion

4.1. Thermal analysis

Optimal processing temperatures, such as the terpolymer annealing temperature, was identified through the second melting scan via DSC measurements. Results are shown in Figure 4 and Table 1.

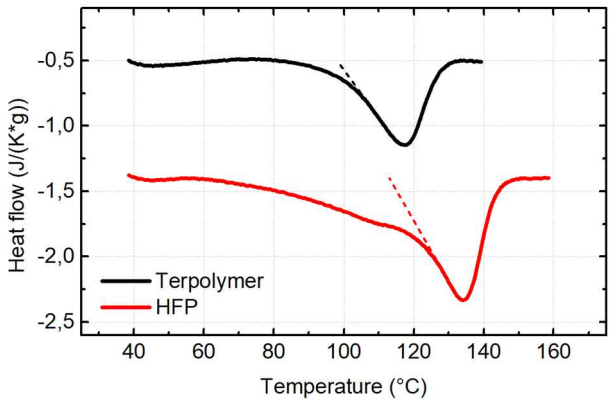

Figure 4. Differential scanning calorimetry (DSC) thermographs of the 2nd melting ramp for the selected polymers: highly polar polyvinylidene fluoride-trifluoroethylene-chlorotrifluoroethylene (PVDF-TrFE-CTFE) terpolymer (black line) and barrier polymer polyvinylidene fluoride-hexafluoropropylene (PVDF-HFP) copolymer (red line).

Table 1. Differential Scanning Calorimetry (DSC) thermal analysis results for the selected polymers.

	$T_{melting}$ °C	T_{onset} °C
Terpolymer	118	98
PVDF-HFP	134	113

As demonstrated in our previous work [80] the most appropriate annealing temperature allowing improvement of the dielectric properties of the PVDF-TrFE-CTFE terpolymer was the one corresponding to the onset of the melting peak, namely 98°C. Such a temperature proved to be high enough for providing sufficient mobility to the molecules to self-organize in crystalline structures while concurrently avoiding melting and melting-driven defects in the polymeric film.

In the case of multilayered samples, the annealing temperature (98°C) was chosen to be equal to one of the terpolymers since the annealing temperature of the PVDF-HFP copolymers was higher (113°C) and would have led to melting of the underlying terpolymer film.

4.2. Morphological characterization

Evaluation of $BaTiO_3$ nanoparticle dispersion and validation of ultrasound stirring protocol was achieved via SEM imaging. Figure 5a and Figure 5b show the cross-section of PVDF-HFP single-layer films doped with 10%$_{vol.}$ and 20%$_{vol.}$ $BaTiO_3$ nanoparticles, respectively. The result confirms good dispersion of the developed composites even with high filler content of 20% vol.

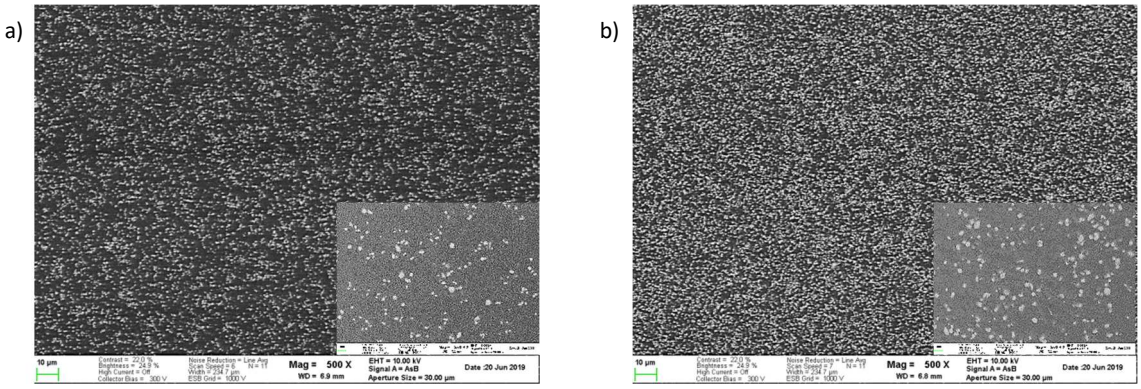

Figure 5. Scanning electron microscopy (SEM) images of cross-section of PVDF-HFP composites films containing a)10%$_{vol.}$ and b) 20%$_{vol.}$ of 500 nm $BaTiO_3$ nanoparticles. Insets show magnifications.

Figure 6 illustrates the cross-section of a multilayered sample achieved after solution casting of PVDF-HFP dissolution on top of a post-annealed terpolymer film (section 2.1). The choice of solvent for film casting of the upper layer (MEK) allowed us to obtain an intimate and homogenous adhesion between the two layers.

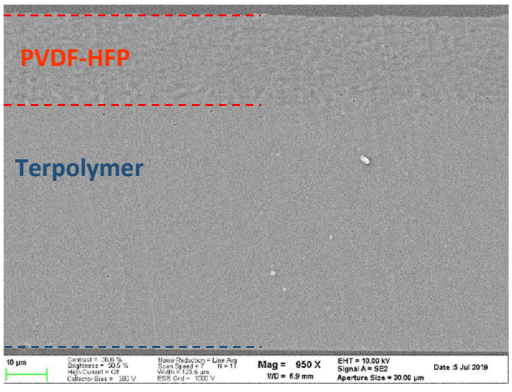

Figure 6. SEM image of "Terpolymer+HFP" multilayer cross-section.

4.3. Electrical characterizations

4.3.1. Single-layer film

Figure 7 illustrates the dielectric permittivity and dielectric strengths of the PVDF-TrFE-CTFE terpolymer, PVDF-HFP copolymers, and their composites doped with 10% and 20% BTO nanoparticles. As observed in Figure 7a, the terpolymer

showed significantly higher permittivity (32 at 1 kHz) with respect to the HFP pure copolymer (7.5 at 1 kHz) under a large frequency range from 0.1 Hz to 1 MHz. Interestingly, the HFP composites consisting of 10%$_{vol.}$ and 20%$_{vol.}$ of $BaTiO_3$ nanoparticles led to a greatly increased permittivity compared to the pure ones. Indeed, the relative permittivity of the HFP10BTO and HFP20BTO increased to 12.7 and 15.8, respectively, at 1 kHz compared to 7.5 as in case of pure HFP. Figure 7b depicts the experimental results (open circles) and the corresponding Weibull model fitting (equation (1)) of the breakdown distribution probability for all materials (solid lines). It can be seen that the HFP copolymer and its composites exhibit a superior breakdown of the electric field when compared with the terpolymer. Incorporating the piezoelectric nanoparticles into the copolymer matrix resulted in a considerably decreased dielectric strength, which was still higher than the terpolymer. The addition of particles in polymeric matrix consists in introduction of several interfaces between the organic and inorganic phases which often represent a preferential pathway of conduction charges [31,66]. Especially in our case, composites made from particles with much higher permittivity than the one of the host polymer leads to dramatically increase local electric fields surrounding particles. This effect results in higher breakdown probability, and thus a degradation of the material dielectric strength [81,82]. In conclusion, the terpolymer and copolymer were complementary rather than competitive. It would therefore be interesting to investigate the multilayered design consisting of these materials so as to efficiently exploit all of their potentials. To some extent, using terpolymers as the main dielectric elements and HFP-based copolymers as thin-barrier layers probably permits the best tradeoff between dielectric properties and electrical breakdown, which is considered to be one of the most relevant characteristics for achieving high electroactive polymer performance.

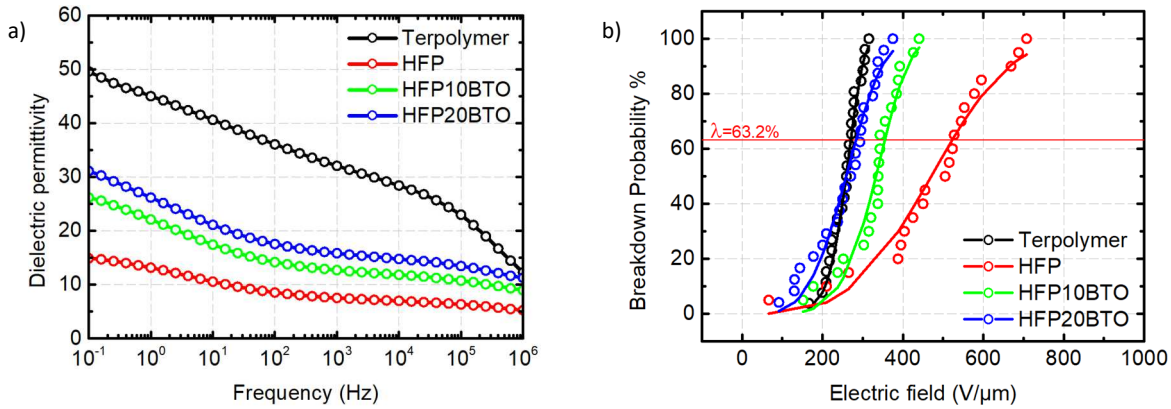

Figure 7. a) Dielectric permittivity versus frequency and b) experimental (circles) and modeled Weibull (solid lines) electric breakdown distribution for selected polymers and composites as single-layer films.

Insulating properties relating to the DC volume resistivity (ρ_{DC}) were compared to the electrical breakdown value (λ) as displayed in Figure 8a. Interestingly, a similar trend of these two parameters was achieved, confirming that implementation of an insulating barrier layer-based PVDF-HFP copolymer gave rise to improved dielectric strength and reduced leakage current, which is mainly caused by the electronic conduction effect. The same result was achieved for the alternative configuration in which the samples were excited by an alternative bipolar voltage corresponding to ±40 V/μm amplitude and 0.1 Hz frequency. As illustrated in Figure 8b, the HFP copolymer led to the highest AC volume resistivity with respect to the other, which was consistent with the result found in Figure 8a. Accordingly, when a large AC or DC electric field was applied, the leakage current through the polymer capacitors was principally affected by electronic conduction and thus, for a target application in either alternative or continuous power, the insulating barrier layers provided enhancement in terms of energy dissipation, dielectric strength, lifetime, and charge–discharge efficiency. A summary of experimental and model results is shown in Table 2.

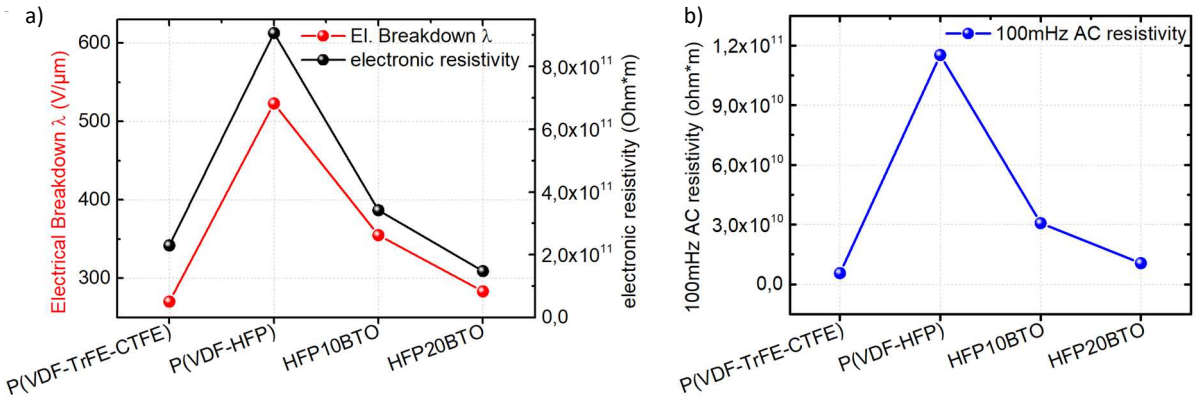

Figure 8. a) Parameter of breakdown electric field (λ) and electronic DC resistivity, and b) AC resistivity for all selected polymers and composites.

Table 2. Electrical characterization results for single-layer capacitors.

	permittivity @ 1kHz	*λ V/µm*	*k*	*DC resistivity Ohm*m*	*AC resistivity Ohm*m*
Terpolymer	32	270	8.35	2.3 x10^{11}	5.6 x10^{9}
HFP	7.5	523	3.47	9.1 x10^{11}	115 x10^{9}
HFP10BTO	12.7	355	5.73	3.4 x10^{11}	30.7 x10^{9}
HFP20BTO	15.8	283	4.05	1.5 x10^{11}	10.6 x10^{9}

The dielectric behavior of pure polymers and of HFP/BTO composites under high AC electric fields of 80 V/µm amplitude and 0.1 Hz frequency was investigated and recorded as the polarization loops of electric displacement (Figure 9a). Due its relaxor-ferroelectric nature, the terpolymer exhibited superior hysteresis behavior over the HFP and its composites [13,83,84]. On the other hand, the pure copolymer displayed a perfectly linear relationship between electric displacement and input voltage excitation without any hysteresis loss. Due to the presence of ferroelectric $BaTiO_3$ nanoparticles, a small amount of hysteresis appeared on the polarization loop of both HFP10BTO and HFP20BTO samples, resulting in a decrease in saturation electric field with respect to the one the pure HFP. Notably, in case of HFP20BTO sample, the electric displacement loop was recorded up to 50 V/µm applied electric field. Indeed, above this value, leakage current ($j_{leakage}^{AC}$) becomes significant, resulting in nonlinear response that would be difficult to be modeled. Within such an electric field range, the conduction current component ($j_{leakage}^{AC}$) can be simply estimated through the Ohm's law, making it possible to accurately determine the purely capacitive response (j_{cap}) as well as the electrical displacement loops of the material (cf. Figure 9a, and equations (3)-(4)). Experimental results revealed that for the other samples (i.e. single-layer terpolymer, HFP and HFP10BTO), a somewhat higher electric field of 80V/µm can be used to get linear behavior. In the next subsection, it will be demonstrated that HFP20BTO when combined with terpolymer to form a multilayer-based structure allows an application of 80 V/µm, which is similar to the one used in the other multilayer samples.

The dielectric permittivity evolution under very high electric field (such as 500 V/µm which is very close, or even higher, than most of polymer/composite breakdown electric fields) based on Debye/Langevin model of equation (6) is illustrated in Figure 9b, which was deduced from the empirical measurement of Figure 9a. Interestingly, the result allowed us to explore the dielectric behavior of the developed materials beyond the crystal saturation electric field (E_{sat}^{θ}). The pure copolymer led to extremely stable permittivity for a large electric field range, reflecting its exceptionally properties in high voltage applications. In contrast, the permittivity of the terpolymer rapidly dropped from 64 to 9 at the higher excitation of 250 V/µm, and its steady value indicated that it was very similar to the one of PVDF-HFP copolymers. Indeed, the terpolymer possessed an amorphous phase very similar to the copolymer's one [85,86], and in general, most of PVDF-based polymers have a large saturation electric field (≈475 V/µm) at which the permittivity is approximately closed to 12 [76]. Similar to the case of HFP composites,

once the saturation electric field was reached, its dielectric permittivity converged to the value of the copolymer matrix. The copolymer doped with piezoelectric particles seems to be the most appropriate candidate to achieve the best tradeoff between the dielectric properties and high voltage application. Fitting parameters are summarized in Table 3 and were in perfect agreement with the literature [76] and our previous results [18,32]. The nomenclature "*matrix*" and "*phase*" adopted in Table 3 is dedicated to the Debye/Langevin model parameters (i.e, $\mathcal{E}_r(0)$ and E_{sat}^{θ}) to each material phase: in case of pure semicrystalline terpolymer (the first line), "*matrix*" refers to the amorphous part and "*phase*" refers to crystalline part; in case of HFP composites (the last two line), such as PVDF-HFP/$BaTiO_3$, "*matrix*" refers the copolymer hosting matrix and "*phase*" to the $BaTiO_3$ particles.

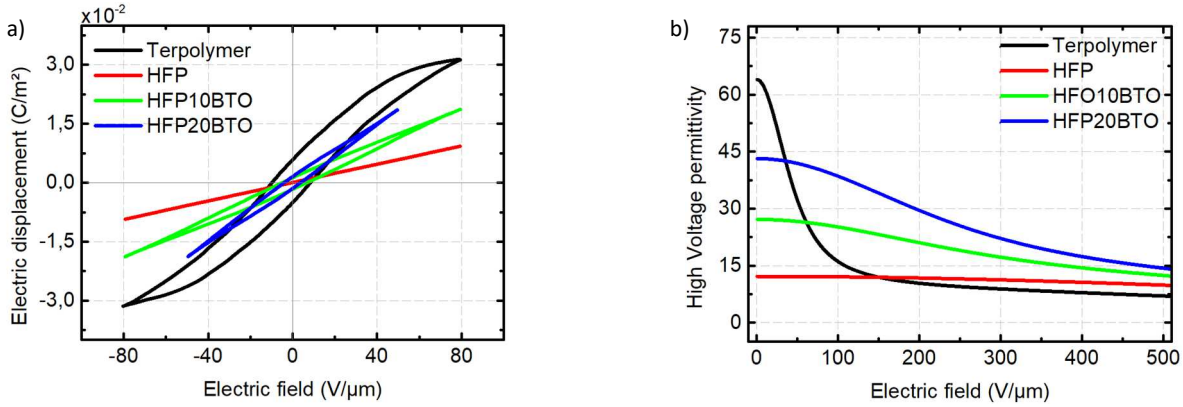

Figure 9. a) Experimental electric displacement, and b) evolution of modelled dielectric permittivity versus applied electric field for all selected polymers and composites.

Table 3. Fitting parameters based Debye/Langevin model. In case of the pure terpolymer (the first line), "matrix" refers to amorphous part and "phase" refers to crystalline part. On the other hand, for the HFP composites (the last two lines), "matrix" refers to the copolymer and "phase" relates to BTO particles.

	$\mathcal{E}_r(0)$	*matrix*		*phase*		$\mathcal{E}_r(E)$
		$\mathcal{E}_r^{\theta}$	E_{sat}^{θ}	$\mathcal{E}_r^{\theta}$	E_{sat}^{θ}	*@ 250 V/µm*
Terpolymer	63.9	10	400	59	21	9.5
HFP	12.2	13.2	475	- -	- -	11.5
HFP10BTO	27.2	13.2	475	16	120	19
HFP20BTO	43.2	13.2	475	32	110	25.5

4.3.2. Multi-layer film capacitor

The structure of multilayered capacitors is schematized in Figure 2 and their fabrication process is described in subsection 2.2. For a better assessment of the fabricated materials, Figure 10 displays the BDS spectra of the single-layer terpolymer and of the single-layer HFP together with the ones of the three multilayered samples including terpolymer+HFP, terpolymer+HFP10BTO, and terpolymer+HFP20BTO. As expected and shown in Figure 10a, the HFP/BTO composite-coated terpolymer gave rise to superior dielectric permittivity as opposed to the one elaborated with pure HFP. Incorporating the piezoelectric particles into the copolymer matrix gave rise to enhanced dielectric properties, which agreed with the result shown in Figure 7a. Interestingly, the permittivity value of the multilayered architecture was situated between one of the single-layers of PVDF-TrFE-CTFE and of single-layer HFP composite. In our next study, we will demonstrate that by combining both terpolymer and copolymer characteristics, it would be possible to obtain high performance multilayered capacitors with better compromise in terms of dielectric property and conduction loss.

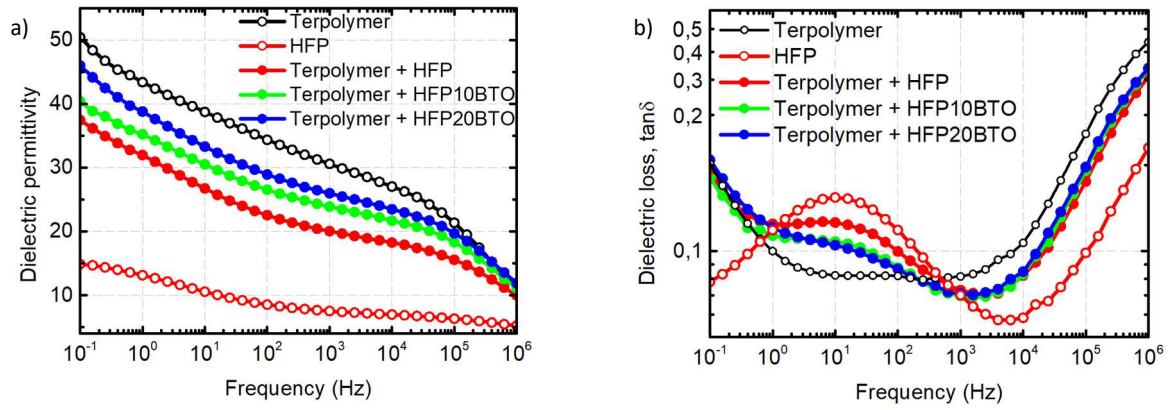

Figure 10. Broadband dielectric spectroscopy (BDS) a) dielectric permittivity spectra and b) dielectric loss spectra for the single-layer terpolymer (open black circles), single-layer HFP (open red circles) and the multilayered capacitors (solid colored circles).

It can be seen in Figure 11 that the multilayered capacitor ($C_{multilayer}$) could be modeled as three capacitors in series, including $C_{barrier}$,, $C_{interface}$, and C_{terpo}. Therefore, $C_{multilayer}$ was calculated using the equation:

$$C_{multilayer} = \left[\frac{1}{C_{terpo}} + \frac{1}{C_{interface}} + \frac{1}{C_{barrier}}\right]^{-1} \quad (12)$$

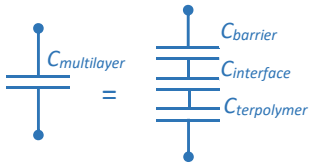

Figure 11. Equivalent model for a multilayered capacitor.

As the thickness of the interface layer was very small compared to the one of the terpolymer and barrier layers, the capacitor value $C_{interface}$ was supposed to be infinite. Thus, the expression of the equivalent capacitor shown in equation (12) could be simplified:

$$C_{multilayer} = \left[\frac{1}{C_{terpo}} + \frac{1}{C_{barrier}}\right]^{-1} \quad (13)$$

Since all layers had the same surfaces, the dielectric permittivity ($\mathcal{E}_{eq}$) of the whole structure deduced from equation (13) was written:

$$\frac{\mathcal{E}_{eq}}{d_{terpo} + d_{barrier}} = \left[\frac{d_{terpo}}{\mathcal{E}_{terpo}} + \frac{d_{barrier}}{\mathcal{E}_{barrier}}\right]^{-1} \quad (14)$$

in which $\mathcal{E}_{terpo}$ and $\mathcal{E}_{barrier}$ refer to the dielectric permittivity of the terpolymer layer and barrier layer, d_{terpo} and $d_{barrier}$ design, respectively, in the thickness of the corresponding layers.

Finally, the theoretical permittivity ($\mathcal{E}_{eq}$) of the whole multilayer structure can be given by the equation:

$$\mathcal{E}_{eq} = \frac{\mathcal{E}_{terpo} \cdot \mathcal{E}_{barrier}}{\mathcal{E}_{barrier} \cdot d_{terpo} + \mathcal{E}_{terpo} \cdot d_{barrier}} (d_{terpo} + d_{barrier}) \quad (15)$$

Table 4 summarizes the experimental (Figure 10a) and theoretical (equation (15)) dielectric permittivity at 1 kHz of the HFP samples in addition to the corresponding absolute ($\mathcal{E}_{exp} - \mathcal{E}_{eq}$) and relative ($\Delta\mathcal{E}\%$) errors.

Table 4. Multilayers dielectric permittivity at 1kHz, experimental (ε_{exp}) and modeled (ε_{eq}) values.

	ε_{exp}	ε_{eq}	$\varepsilon_{exp} - \varepsilon_{eq}$	$\Delta\varepsilon\%$
Terpolymer	32			
Terpolymer+HFP	20.4	19.4	+1	5%
Terpolymer+HFP10BTO	23.9	24.5	-0.6	2.5%
Terpolymer+HFP20BTO	26	26.6	-0.6	2.3%

The permittivity constant of all materials at 1 kHz allowed us to assess their dielectric properties originating from the polarization mechanisms that was principally due to dipolar/molecular interactions. However, these characteristics were not affected by interfacial and/or conductive phenomena (such as ionic or DC conductivity) that occurred at much lower frequency (as shown in Figure 10b). The small discrepancy between the experimental and theoretical values of permittivity, such as ε_{exp}-ε_{eq} as reported in Table 4, allowed us to conclude that under low voltage excitation, the introduced interface between the terpolymer and the barrier layers did not alter the dielectric behavior of the whole multilayered structure. Observing the BDS spectra in Figure 10b, the dielectric loss spectra of the single-layer HFP and of the multilayered samples exhibit a peak at medium frequency range (i.e. around 10Hz), and this observation does not appear in the case of the single-layer terpolymer. On the other hand, the single layer copolymer (open red circles) leads to the most important peak, which gradually decreases in the case of bilayer films containing terpolymer layer and HFP composite layer. This decrease is more obvious with increasing particles content inside the composite layer, which is confirmed by evolution of the three solid-circle curves depicted on Figure 10b. The obtained result can be explained by the fact that for the pure PVDF-HFP copolymer, the related relaxation phenomenon probably infers to interfacial polarization at the level of crystalline/amorphous interfaces [48,87,88]. Introduction of inorganic particles (such as $BaTiO_3$) may leads to reduced crystallinity and thus lower contribution of interfacial polarization to the loss peak at ≈10Hz. Moreover, it was observed in Figure 10b that toward low frequencies (< 1Hz), the dielectric loss spectrum of all multilayered samples displayed a similar trend as seen in one of the single-layer terpolymers, confirming that the interface between the adjacent layers did not induce any parasitic polarization mechanism.

Charge–discharge cycles were applied with a bipolar AC voltage at 0.1 Hz frequency and 80 V/µm amplitude. The measured currents of the single-layer terpolymer and of the three multilayered materials are represented in Figure 12a in which straight dashed lines describe the leakage current through the capacitor-like samples. As the charge–discharge cycles are symmetrical as a function of the sign of both current density and electric field, magnification of the leakage currents is shown only for the first quarter in Figure 12b. The linear trend of the leakage current versus the applied electric field for each sample depicted a linear resistive behavior according to the Ohm's law as shown in equation (2). The results highlight that the introduction of an insulating barrier layer could lead to successful control of conduction losses. In other words, an additional layer of 15 µm of pure PVDF-HFP layer permitted leakage current reduction at high voltage application by almost 70%. Actually, the volume resistivity (ρ_{AC}) increased from 5.6×10^9 ohm*m for the single-layer terpolymer to 18.5×10^9 ohm*m for the multilayered Terpolymer+HFP, corresponding to a three-fold improvement in terms of conduction losses. The multilayered capacitors based on HFP composites led to higher leakage currents than the ones embedded with the pure HFP but were still lower than the single-layer terpolymers. Table 5 shows the volume resistivity value of the four samples, estimated from the slopes represented in Figure 12b.

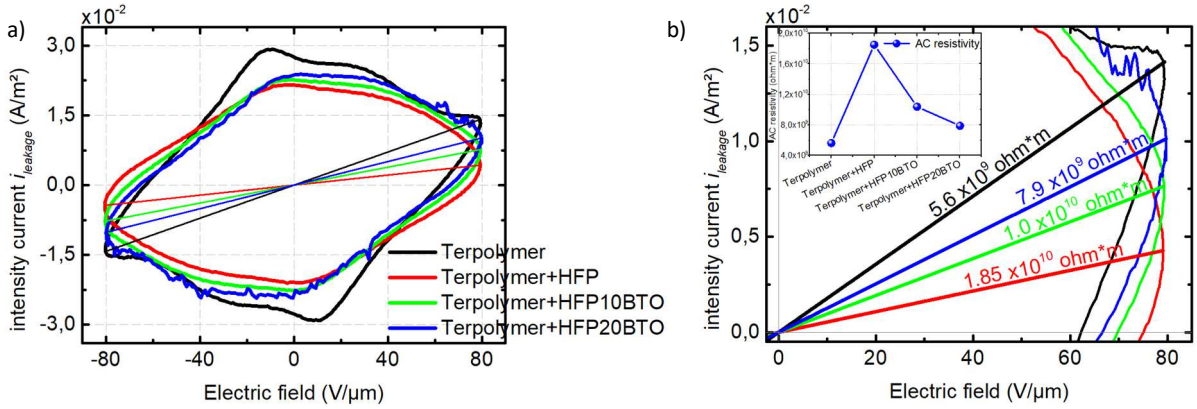

Figure 12. a) Charge–discharge current for a single-layer terpolymer (black line) and for all multilayered capacitors (colored lines). b) Magnification of the first quarter with positive values of current and electric field: straight lines feature the leakage currents intensity and relative volume resistivity; the inset depicts the trend of volume resistivity of each multilayered capacitor.

Figure 13a illustrates the electric displacement deduced from the integral of the capacitive current (equation (4)) versus the applied electric field of the single-layer terpolymer and of all of the multilayered capacitors. To make observations easier, Figure 13b only displays the first quarter of the polarization loop. It can be seen that under the same electric field of 80 V/µm, the maximum polarization level (P_{max}) of the three multilayers was slightly lower than the one of the single-layer terpolymer (a reduction of ≈11%, 6%, 2% for the Terpolymer+HFP, Terpolymer+HFP10BTO, and Terpolymer+HFP20BTO, respectively). This deterioration was considered to be negligible with respect to conduction losses enhancement of the three corresponding multilayers whose volume resistivity drastically increases of 70%, 44%, and 29% (Table 5). As previously mentioned in subsection 4.3.1, the PVDF-HFP possesses a liner dielectric behavior ($\mathcal{E}_r \approx 13$) with large polarizability even under a high electrical field. In Figure 12a, the current response of the single-layer terpolymer (solid black curve) shows the typical features of a relaxor-ferroelectric polymer where four peaks are visible and discernible. Concerning the multilayered samples, the linear dielectric PVDF-HFP layer (as measured in Figure 9a) leads to current response curves in which the peaks are broaden and partially merged, confirming a linearization of the overall dielectric response of the multilayered samples. Actually, in such architecture where two layers are in series, the measured resulting current (Figure 12a) is the sum of the current response of each layer. Hence, the relaxor-ferroelectric features of the terpolymer are partially covered up by the linear dielectric response of the PVDF-HFP layer (in case of Terpolymer+HFP) and by the normal-ferroelectric response of PVDF-HFP/$BaTiO_3$ composites layer (in case of Terpolymer+HFP10BTO, and Terpolymer+HFP20BTO). These interesting properties make a possibility to fabricate multilayered structures with quasi-zero ferroelectric losses ($P_r \approx 0$) at a given applied electric field (e.g. 80 V/µm); These interesting properties presented the possibility of fabricating multilayered structures with quasi-zero ferroelectric losses ($P_r \approx 0$) at the tested applied electric field (80 V/µm); as in the case of the conventional PVDF-HFP copolymer, the three multilayered configurations coated with HFP, HFP10BTO, and HFP20BTO led to substantially decreased remnant polarization (P_r) of around 90%, 80%, and 70%, respectively, as opposed to the single-layer terpolymer. In conclusion, multilayered design based HFP/$BaTiO_3$ composites led to the best tradeoff between conduction/ferroelectric losses (Figure 12b) and charge displacement (Figure 13b) in which the maximum polarization level was almost unchanged and close to the one of the classical terpolymer PVDF-TrFE-CTFE.

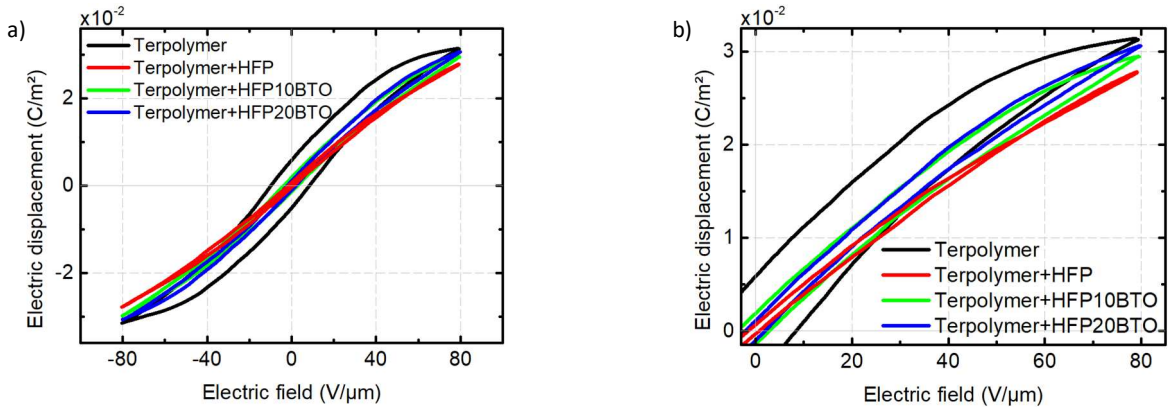

Figure 13. a) Electric displacement versus applied electric field for single-layer terpolymer (black line) and for all multilayered capacitors (colored lines); b) Magnification of first quarter corresponding to positive values of electric displacement and electric field.

Table 5. Multilayer AC volume resistivity ρ_{AC} and material polarization properties.

	*AC resistivity, ρ_{AC} Ohm*m*	*$\Delta\rho_{AC}$ %*	*Remnant polarization, P_r C/m²*	*ΔP_r %*	*Polarization max, P_{max} C/m²*	*ΔP_{max} %*
Terpolymer	5.6 x10^9		5.9 x10^{-3}		3.13 x10^{-2}	
Terpolymer+HFP	18.5 x10^9	+ 70%	0.6 x10^{-3}	- 88.5%	2.76 *x10*$^{-2}$	- 11.3%
Terpolymer+HFP10BTO	10 x10^9	+ 44%	1.1 x10^{-3}	- 81.2%	2.95 x10^{-2}	-5.8%
Terpolymer+HFP20BTO	7.9 x10^9	+ 29%	1.9 x10^{-3}	- 67.2%	3.06 x10^{-2}	-2.2%

In order to estimate the energy-storage efficiency (η) previously defined in equation (9), the electric displacement loops were then calculated from the integral of the experimental current (J_{tot}) written in equation (3). The total electric displacement loops are displayed in Figure 14a while the corresponding energy-storage densities in terms of total stored energy (U_{stored}) and recovered energy ($U_{recovered}$) are reported in Figure 14b for all fabricated samples. The total stored energy density (U_{stored}) contains both the recoverable energy density $U_{recovered}$ (cf. green area in Figure 3) and the energy dissipations U_{loss} (cf. red area in Figure 3). Energy losses principally stem from conduction current, ferroelectric losses, and relaxation modes dedicated to molecular dipole orientation, that occurred during electric solicitation of polymer. At a given applied electric field of 80V/µm, the stored energy density (U_{stored}) of the single-layer terpolymer is significantly superior to the other multilayered samples, i.e. 2.51 J/cm^3 with respect to 1.44 J/cm^3 as in the case of the Terpolymer+HFP multilayer. On the other hand, the recoverable energy density ($U_{recovered}$) of the Terpolymer+HFP reaches the maximum value compared to the other materials (i.e. from 0.67 J/cm^3 down to 0.42 J/cm^3), making it as the best candidate to achieve the most optimal energy-storage efficiency (η) as reported on Figure 15.

The results reveal that the Terpolymer+HFP multilayer gave rise to more than a two-fold increase in energy-storage efficiency as opposed to the conventional terpolymer (from 20% to 47%), which can be explained by the fact that the PVDF-HFP copolymer allowed for successfully reduction of both conduction and ferroelectric losses. On the other hand, the other multilayers based on HFP composite solutions did not show significant enhancement for the ultimate capacitor efficiency despite their boosted polarization properties. Concretely, the barrier layer carried out with 10%$_{vol.}$ $BaTiO_3$ resulted in a slight increase in energy-storage efficiency of 7% with respect to the single terpolymer film. Nonetheless, the multilayered samples with higher filler content of $BaTiO_3$ (20%$_{vol.}$) achieved an ultimate capacitor efficiency of 19%, which was even lower than the one with the terpolymer material. These results, together with the AC volume resistivity of the multilayered structures shown in Figure 12b, emphasized the predominance of conduction losses (or leakage current) above all other dissipation mechanisms. As observed, values of energy-storage efficiency in Figure 15 followed the same trend as AC resistivity (depicted in the inset of Figure 12b).

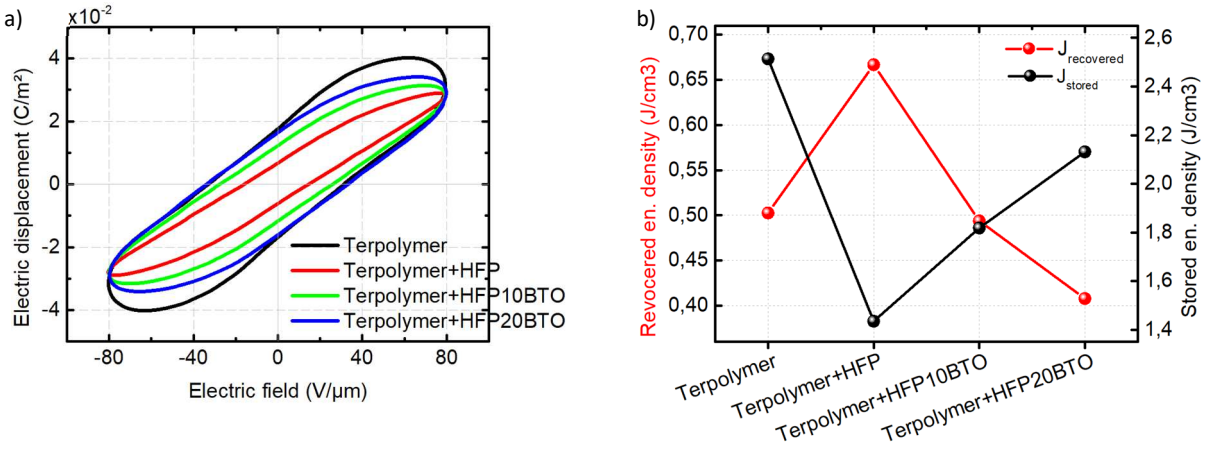

Figure 14. a) Charge–discharge electric displacement loops for single-layer terpolymer (black line) and for all multilayered capacitors (colored lines), and b) recoverable energy density ($J_{recovered}$) and total stored energy density (J_{stored}) values for all fabricated samples measured at 80V/μm.

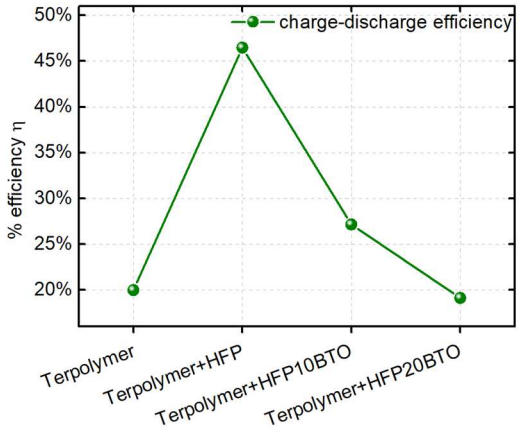

Figure 15. Energy-storage efficiency (η) for single-layer terpolymer and for all multilayered capacitors measured at 80V/μm.

It is noteworthy that the energy-storage efficiency of our film capacitors is not ideal compared to those reported in the literature [38,59–61] because of conduction losses in energy dissipation, as previously discussed. The selected barrier material, i.e PVDF-HFP, besides the higher insulating properties, still belongs to the same class of PVDF-TrFE-CTFE terpolymers which is characterized by high permittivity thanks to additional molecular-dipole polarization. This mechanism creates, simultaneously, higher level of conduction losses, the so-called leakage current. An alternative method to further improve the energy efficiency consists in using highly insulating materials as barrier layers such as high-glass transition polymers (e.g. PC). At the same time, highly insulating materials generally show small values of dielectric permittivity which, at low electric fields, relevantly limits the maximum polarization response. Moreover, when comparing electrical properties of different polymer systems, it is important to pay attention at the nominal thickness of the samples since its relevance in the polymer breakdown electric field [89–91]. Notably, with respect to multilayered polymeric capacitors often reported in literature, our fabricated samples possess values of thickness from 5 to 15 times larger. Fabrication of thinner polymeric films, together with the reduction of the probability to encounter defects for a given electrode area [92], results in more homogenous samples as other relevant fabrication parameters are affected such as heat dissipation and solvent evaporation rate [93,94].

Finally, the dielectric strength of all multilayered samples was tested, and the breakdown probability distribution is illustrated in Figure 17. The experimental breakdown electric field distribution was fitted into the Weibull model defined in equation (1) and whose fitting parameters, λ and k, are reported in Table 6. As expected, the addition of a thin barrier layer of pure copolymer

makes it possibility to build a multilayered capacitor with enhanced dielectric strength. It was previously clarified in subsection 4.3.1 that high voltage failures are directly related to the magnitude of electronic conductivity through the polymeric capacitor (Figure 8a). The introduction of a copolymer layer capable of acting as a barrier against electron flux led to lower leakage current in addition to improved breakdown electric field. Moreover, after considering multilayered structures as a series of capacitors that were excited by an input voltage (V_{tot}), it can be seen that the electric field was redistributed internally among the layers somehow depending on the permittivity value of each layer [60,95]. Assuming the electric displacement between terpolymer layer and barrier layer interface being continuous, the values of internal electric field in each layer could be estimated:

$$D(E) = \mathcal{E}_{terpo}(E) \cdot E_{terpo} = \mathcal{E}_{barrier}(E) \cdot E_{barrier} \tag{16}$$

In which $\mathcal{E}_{terpo}$ and $\mathcal{E}_{barrier}$ denote the permittivity of terpolymer and barrier material, respectively. The internal electric fields E_{terpo} and $E_{barrier}$ in each layer could be expressed:

$$E_{terpo} = V_{tot} \frac{1}{d_{barrier} \frac{\mathcal{E}_{terpo}(E)}{\mathcal{E}_{barrier}(E)} + d_{terpo}} \tag{17}$$

$$E_{barrier} = V_{tot} \frac{1}{d_{terpo} \frac{\mathcal{E}_{barrier}(E)}{\mathcal{E}_{terpo}(E)} + d_{barrier}} \tag{18}$$

Equations (17) and (18) demonstrate that the internal electric field is inversely proportional to permittivity, meaning that material with smaller permittivity absorbed a greater portion of electrical energy. In case of the Terpolymer+HFP multilayer, when the applied voltage was close to the breakdown level (> 250 V/μm), the permittivity of terpolymer almost equaled the one of the copolymer (as illustrated in Figure 9b). This effect, highlighted in Figure 16a, led to homogeneous electric field redistribution across the layers and resulted in boosted breakdown strength for the Terpolymer+HFP multilayer whose λ parameter attained the maximum value as shown in Table 6. In contrast, in cases of other multilayers, such as Terpolymer+HFP10BTO and Terpolymer+HFP20BTO, the composite layers exhibited much higher permittivity values than those of the underlying terpolymer under the same high voltage condition (Figure 9b). This makes the "weak" terpolymer layer subjected to the larger portion of the electric field (see Figure 16b and Figure 16c) together with imbalanced electric field redistribution through the whole sample, resulting in earlier breakdown as confirmed by the experimental measurements shown in Figure 17.

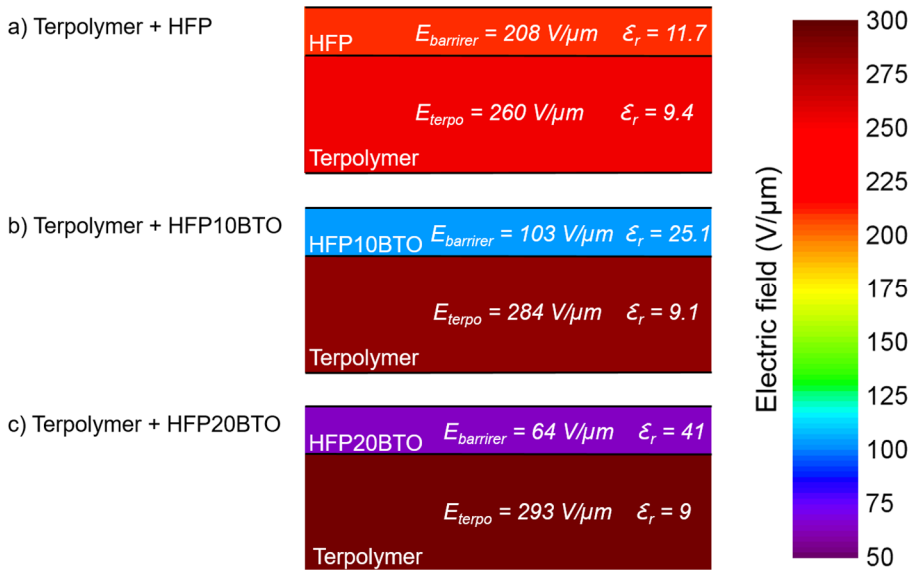

Figure 16. Representation of electric field redistribution internally to each layer of the multilayered capacitor structures, for a given applied electric field of 250 V/µm: a) Terpolymer+HFP, b) Terpolymer+HFP10BTO and c) Terpolymer+HFP20BTO.

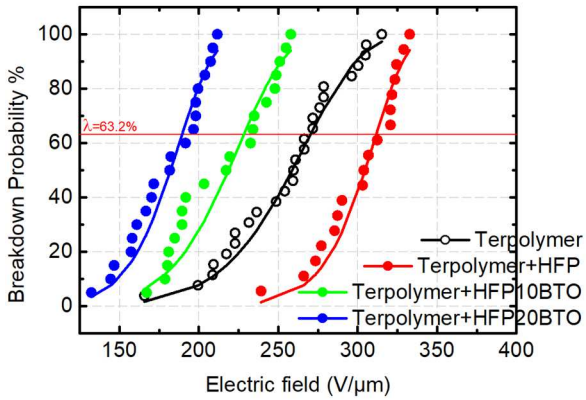

Figure 17. Experimental breakdown distribution for single-layer terpolymer (open black circles) and for all multilayered capacitors (solid colored circles). Lines represent the modeled Weibull breakdown probability.

Table 6. Multilayer dielectric strength by Weibull analysis and multilayer capacitor efficiencies.

	λ V/µm	*Δλ* %	*k*	*energy-storage efficiency, η @ 80 V/µm*
Terpolymer	270		8.35	20.0%
Terpolymer+HFP	312	+ 16%	15.95	46.5%
Terpolymer+HFP10BTO	228	–16%	8.49	27.2%
Terpolymer+HFP20BTO	190	–30%	9.34	19.1%

5. Conclusions

This paper proposed a simple and straightforward technique for elaboration of polymeric film capacitors. The alternative fabrication process involves in realization of bilayer film capacitors via solution-casting (or doctor-blading), a versatile and

costless deposition technique which, together with the right solvent choice, allows to finely tune the thickness of each deposited layers. The novel architecture consists in adding a thin barrier layer on the top of a main dielectric polymer in order to substantially lower the conduction losses. The well-known relaxor-ferroelectric PVDF-TrFE-CTFE terpolymer with exceptional dielectric properties was chosen as the main dielectric layer, whereas the highly polar PVDF-HFP copolymer was dedicated as the barrier layer. This new capacitor design allowed us to achieve high-performance bilayer material with boosted energy-storage efficiency up to almost 50% as opposed to the traditional single-layer PVDF-TrFE-CTFE terpolymer. Also, the implemented thin barrier layer effectively prevented around 70% electric conduction losses, thus giving rise to enhanced dielectric strength in addition to enhancing the lifetime of electronic devices. Finally, the barrier layer contributed to the extinction of ferroelectric losses (approximately 90%) inherent in the relaxor-ferroelectric PVDF-TrFE-CTFE terpolymer, making it possible to overcome the main technological challenges, such as high leakage current and breakdown electric field, found in most organic materials.

6. Acknowledgements

This work was supported by SOLVAY, ANRT, and INSTITUT CARNOT. I am deeply thankful to Engineer Nicolas Uguen for the fruitful scientific discussions concerning polymer nanocomposites and dielectric losses.

7. References

[1] Q. Tan, P. Irwin, Y. Cao, Advanced Dielectrics for Capacitors, IEEJ Trans. Fundam. Mater. 126 (2006) 1153–1159. https://doi.org/10.1541/ieejfms.126.1153.

[2] TRS Technologies, Inc., (n.d.) http://www.trsceramics.com. http://www.trsceramics.com (accessed November 13, 2019).

[3] T.R. Jow, F.W. Macdougall, J.B. Ennis, X.H. Yang, M.A. Schneider, C.J. Scozzie, J.D. White, J.R. Macdonald, M.C. Schalnat, R.A. Cooper, S.P.S. Yen, Pulsed power capacitor development and outlook, Dig. Tech. Pap. Int. Pulsed Power Conf. 2015-Octob (2015). https://doi.org/10.1109/PPC.2015.7297027.

[4] B. Wang, W. Huang, L. Chi, M. Al-Hashimi, T.J. Marks, A. Facchetti, High- k Gate Dielectrics for Emerging Flexible and Stretchable Electronics, Chem. Rev. 118 (2018) 5690–5754. https://doi.org/10.1021/acs.chemrev.8b00045.

[5] I. Rytöluoto, K. Lahti, M. Karttunen, M. Koponen, Large-area dielectric breakdown performance of polymer films - Part i: Measurement method evaluation and statistical considerations on area-dependence, IEEE Trans. Dielectr. Electr. Insul. 22 (2015) 689–700. https://doi.org/10.1109/TDEI.2015.7076764.

[6] Y. Zhu, P. Jiang, Z. Zhang, X. Huang, Dielectric phenomena and electrical energy storage of poly(vinylidene fluoride) based high-k polymers, Chinese Chem. Lett. 28 (2017) 2027–2035. https://doi.org/10.1016/j.cclet.2017.08.053.

[7] S.K. Kumar, B.C. Benicewicz, R.A. Vaia, K.I. Winey, 50th Anniversary Perspective: Are Polymer Nanocomposites Practical for Applications?, Macromolecules. (2017). https://doi.org/10.1021/acs.macromol.6b02330.

[8] K. Thetpraphi, M.Q. Le, A. Houachtia, P.J. Cottinet, L. Petit, D. Audigier, J. Kuhn, G. Moretto, J.F. Capsal, Surface Correction Control Based on Plasticized Multilayer P(VDF-TrFE-CFE) Actuator—Live Mirror, Adv. Opt. Mater. 1900210 (2019) 1–7. https://doi.org/10.1002/adom.201900210.

[9] H.G. Kassa, L. Nougaret, R. Cai, A. Marrani, B. Nysten, Z. Hu, A.M. Jonas, The Ferro- to Paraelectric Curie Transition of a Strongly Confined Ferroelectric Polymer, Macromolecules. 47 (2014) 4711–4717. https://doi.org/10.1021/ma500969m.

[10] J. DeGraff, R. Liang, M.Q. Le, J.F. Capsal, F. Ganet, P.J. Cottinet, Printable low-cost and flexible carbon nanotube buckypaper motion sensors, Mater. Des. 133 (2017) 47–53. https://doi.org/10.1016/j.matdes.2017.07.048.

[11] Z. Xiang, B. Ducharne, N. Della Schiava, J.F. Capsal, P.J. Cottinet, G. Coativy, P. Lermusiaux, M.Q. Le, Induction heating-based low-frequency alternating magnetic field: High potential of ferromagnetic composites for medical applications, Mater. Des. 174 (2019) 107804. https://doi.org/10.1016/j.matdes.2019.107804.

[12] M. Streibl, R. Karmazin, R. Moos, Materials and applications of polymer films for power capacitors with special respect to nanocomposites, IEEE Trans. Dielectr. Electr. Insul. (2018). https://doi.org/10.1109/TDEI.2018.007392.

[13] L. Yang, X. Li, E. Allahyarov, P.L. Taylor, Q.M. Zhang, L. Zhu, Novel polymer ferroelectric behavior via crystal isomorphism and the nanoconfinement effect, Polym. (United Kingdom). (2013). https://doi.org/10.1016/j.polymer.2013.01.035.

[14] M. Lallart, K. Thetpraphi, J.F. Capsal, Analysis of temperature effect in dielectric response of electrostrictive polymers for pseudo-pyroelectric operations, Phys. Lett. Sect. A Gen. At. Solid State Phys. 382 (2018) 449–454. https://doi.org/10.1016/j.physleta.2017.12.030.

[15] Q. Liu, X. Yin, C. Richard, J.F. Capsal, Influence of the crystallization on the molecular mobility and ionic DC conductivity behaviors of relaxor ferroelectric P(VDF-TrFE-CTFE) terpolymers, J. Polym. Sci. Part B Polym. Phys. 54 (2016) 1645–1657. https://doi.org/10.1002/polb.24068.

[16] M.R. Gadinski, Q. Li, G. Zhang, X. Zhang, Q. Wang, Understanding of relaxor ferroelectric behavior of poly(vinylidene fluoride-trifluoroethylene-chlorotrifluoroethylene) terpolymers, Macromolecules. 48 (2015) 2731–2739. https://doi.org/10.1021/acs.macromol.5b00185.

[17] N. Della Schiava, M.-Q. Le, J. Galineau, F. Domingues Dos Santos, P.-J. Cottinet, J.-F. Capsal, Influence of Plasticizers on the Electromechanical Behavior of a P(VDF-TrFE-CTFE) Terpolymer: Toward a High Performance of Electrostrictive Blends, J. Polym. Sci. Part B Polym. Phys. 55 (2017) 355–369. https://doi.org/10.1002/polb.24280.

[18] F. Pedroli, A. Marrani, M.-Q. Le, C. Froidefond, P.-J. Cottinet, J.-F. Capsal, Processing optimization: A way to improve the ionic conductivity and dielectric loss of electroactive polymers, J. Polym. Sci. Part B Polym. Phys. 56 (2018) 1164–1173. https://doi.org/10.1002/polb.24636.

[19] X. Hu, K. Yi, J. Liu, B. Chu, High Energy Density Dielectrics Based on PVDF-Based Polymers, Energy Technol. 6 (2018) 849–864. https://doi.org/10.1002/ente.201700901.

[20] D. Wang, Y. Bao, J. Zha, J. Zhao, Z. Dang, G. Hu, Improved Dielectric Properties of Nanocomposites Based on Poly (vinylidene fl uoride) and Poly (vinyl alcohol) -Functionalized Graphene, (2012).

[21] C. Pecharromán, J.S. Moya, Experimental evidence of a giant capacitance in insulator-conductor composites at the percolation threshold, Adv. Mater. 12 (2000) 294–297. https://doi.org/10.1002/(SICI)1521-4095(200002)12:4<294::AID-ADMA294>3.0.CO;2-D.

[22] P. Barber, S. Balasubramanian, Y. Anguchamy, S. Gong, A. Wibowo, H. Gao, H.J. Ploehn, H.C. Zur Loye, Polymer composite and nanocomposite dielectric materials for pulse power energy storage, 2009. https://doi.org/10.3390/ma2041697.

[23] A.B. Da Silva, M. Arjmand, U. Sundararaj, R.E.S. Bretas, Novel composites of copper nanowire/PVDF with superior dielectric properties, Polymer (Guildf). 55 (2014) 226–234. https://doi.org/10.1016/j.polymer.2013.11.045.

[24] M.F. Lin, V.K. Thakur, E.J. Tan, P.S. Lee, Dopant induced hollow BaTiO3nanostructures for application in high performance capacitors, J. Mater. Chem. 21 (2011) 16500–16504. https://doi.org/10.1039/c1jm12429c.

[25] Z.M. Dang, J.K. Yuan, J.W. Zha, T. Zhou, S.T. Li, G.H. Hu, Fundamentals, processes and applications of high-permittivity polymer-matrix composites, Prog. Mater. Sci. 57 (2012) 660–723. https://doi.org/10.1016/j.pmatsci.2011.08.001.

[26] J. Huang, H. Zheng, Z. Chen, Q. Gao, N. Ma, P. Du, Percolative ceramic composites with giant dielectric constants and low dielectric losses, J. Mater. Chem. 19 (2009) 3909–3913. https://doi.org/10.1039/b820815h.
[27] N. Yousefi, X. Sun, X. Lin, X. Shen, J. Jia, B. Zhang, B. Tang, M. Chan, J.K. Kim, Highly aligned graphene/polymer nanocomposites with excellent dielectric properties for high-performance electromagnetic interference shielding, Adv. Mater. 26 (2014) 5480–5487. https://doi.org/10.1002/adma.201305293.
[28] R.C. Smith, C. Liang, M. Landry, J.K. Nelson, L.S. Schadler, The mechanisms leading to the useful electrical properties of polymer nanodielectrics, IEEE Trans. Dielectr. Electr. Insul. 15 (2008) 187–196. https://doi.org/10.1109/T-DEI.2008.4446750.
[29] Q. Li, F.-Z. Yao, Y. Liu, G. Zhang, H. Wang, Q. Wang, High-Temperature Dielectric Materials for Electrical Energy Storage, Annu. Rev. Mater. Res. 483 (2018) 1–325. https://doi.org/10.1146/annurev-matsci-070317.
[30] J.I. Roscow, C.R. Bowen, D.P. Almond, Breakdown in the Case for Materials with Giant Permittivity?, ACS Energy Lett. (2017) 2264–2269. https://doi.org/10.1021/acsenergylett.7b00798.
[31] Y. Thakur, T. Zhang, C. Iacob, T. Yang, J. Bernholc, L.Q. Chen, J. Runt, Q.M. Zhang, Enhancement of the dielectric response in polymer nanocomposites with low dielectric constant fillers, Nanoscale. 3 (2017). https://doi.org/10.1039/C7NR01932G.
[32] F. Pedroli, A. Marrani, M.-Q. Le, O. Sanseau, P.-J. Cottinet, J.-F. Capsal, Reducing leakage current and dielectric losses of electroactive polymers through electro-annealing for high-voltage actuation, RSC Adv. 9 (2019) 12823–12835. https://doi.org/10.1039/C9RA01469A.
[33] W. Sarjeant, Capacitors, IEEE Trans. Electr. Insul. 25 (1990) 861–922. https://doi.org/10.1109/14.59866.
[34] J. Chen, Y. Wang, Q. Yuan, X. Xu, Y. Niu, Q. Wang, H. Wang, Multilayered ferroelectric polymer films incorporating low-dielectric-constant components for concurrent enhancement of energy density and charge–discharge efficiency, Nano Energy. 54 (2018) 288–296. https://doi.org/10.1016/j.nanoen.2018.10.028.
[35] J.C. Fothergill, Electrical Degradation and Breakdown in Polymers, Institution of Engineering and Technology, 1992. http://digital-library.theiet.org/content/books/cs/pbed009e.
[36] N. Grossiord, J.M. Kroon, R. Andriessen, P.W.M. Blom, Degradation mechanisms in organic photovoltaic devices, Org. Electron. Physics, Mater. Appl. 13 (2012) 432–456. https://doi.org/10.1016/j.orgel.2011.11.027.
[37] Q.D. Ling, D.J. Liaw, C. Zhu, D.S.H. Chan, E.T. Kang, K.G. Neoh, Polymer electronic memories: Materials, devices and mechanisms, Prog. Polym. Sci. 33 (2008) 917–978. https://doi.org/10.1016/j.progpolymsci.2008.08.001.
[38] J. Jiang, Z. Shen, J. Qian, Z. Dan, M. Guo, Y. Lin, C.W. Nan, L. Chen, Y. Shen, Ultrahigh discharge efficiency in multilayered polymer nanocomposites of high energy density, Energy Storage Mater. (2018). https://doi.org/10.1016/j.ensm.2018.09.013.
[39] M. Mackey, D.E. Schuele, L. Zhu, L. Flandin, M.A. Wolak, J.S. Shirk, A. Hiltner, E. Baer, Reduction of dielectric hysteresis in multilayered films via nanoconfinement, Macromolecules. (2012). https://doi.org/10.1021/ma202267r.
[40] D. Kuang, R. Li, J. Pei, Polyamide 11/poly(vinylidene fluoride)/vinyl acetate-maleic anhydride copolymer as novel blends flexible materials for capacitors, Polymers (Basel). 6 (2014) 2146–2156. https://doi.org/10.3390/polym6082146.
[41] M.S. Zheng, J.W. Zha, Y. Yang, P. Han, C.H. Hu, Y.Q. Wen, Z.M. Dang, Polyurethane induced high breakdown strength and high energy storage density in polyurethane/poly(vinylidene fluoride) composite films, Appl. Phys. Lett. 110 (2017). https://doi.org/10.1063/1.4989579.
[42] J.-K. Yuan, S.-H. Yao, A. Sylvestre, J. Bai, Biphasic Polymer Blends Containing Carbon Nanotubes: Heterogeneous Nanotube Distribution and Its Influence on the Dielectric Properties, J. Phys. Chem. C. 116 (2012) 2051–2058. https://doi.org/10.1021/jp210872w.
[43] W. Li, L. Jiang, X. Zhang, Y. Shen, C.W. Nan, High-energy-density dielectric films based on polyvinylidene fluoride and aromatic polythiourea for capacitors, J. Mater. Chem. A. 2 (2014) 15803–15807. https://doi.org/10.1039/c4ta03374d.
[44] J. Zhao, X. Yin, J. Shi, X. Zhao, X. Wang, M. Chen, Z.-M. Dang, G.-H. Hu, Effect of the Mixing on the Dielectric Constant of Poly(vinylidene fluoride)/Isotactic Polypropylene Blends, Sci. Adv. Mater. 5 (2013) 505–511. https://doi.org/10.1166/sam.2013.1481.
[45] Z.-M. Dang, W.-T. Yan, H.-P. Xu, Novel high-dielectric-permittivity poly(vinylidene fluoride)/polypropylene blend composites: The influence of the poly(vinylidene fluoride) concentration and compatibilizer, J. Appl. Polym. Sci. 105 (2007) 3649–3655. https://doi.org/10.1002/app.26447.
[46] X. Zhao, J. Zhao, J.P. Cao, X. Wang, M. Chen, Z.M. Dang, Tuning the dielectric properties of polystyrene/poly(vinylidene fluoride) blends by selectively localizing carbon black nanoparticles, J. Phys. Chem. B. 117 (2013) 2505–2515. https://doi.org/10.1021/jp310021r.
[47] K. Yu, Y. Bai, Y. Zhou, Y. Niu, H. Wang, Poly(vinylidene fluoride) polymer based nanocomposites with enhanced energy density by filling with polyacrylate elastomers and BaTiO3 nanoparticles, Appl. Phys. Lett. 104 (2014). https://doi.org/10.1063/1.4866585.
[48] J. Mijovic, J. Sy, T. Kwei, Reorientational dynamics of dipoles in poly (vinylidene fluoride)/poly (methyl methacrylate)(PVDF/PMMA) blends by dielectric spectroscopy, Macromolecules. 9297 (1997) 3042–3050. http://pubs.acs.org/doi/abs/10.1021/ma961774w.
[49] S.J. Kang, Y.J. Park, I. Bae, K.J. Kim, H.C. Kim, S. Bauer, E.L. Thomas, C. Park, Printable ferroelectric PVDF/PMMA blend films with ultralow roughness for low voltage non-volatile polymer memory, Adv. Funct. Mater. 19 (2009) 2812–2818. https://doi.org/10.1002/adfm.200900589.
[50] B. Luo, X. Wang, H. Wang, Z. Cai, L. Li, P(VDF-HFP)/PMMA flexible composite films with enhanced energy storage density and efficiency, Compos. Sci. Technol. 151 (2017) 94–103. https://doi.org/10.1016/j.compscitech.2017.08.013.
[51] F. Liu, Z. Li, Q. Wang, C. Xiong, High breakdown strength and low loss binary polymer blends of poly(vinylidene

fluoride-trifluoroethylene-chlorofluoroethylene) and poly(methyl methacrylate), Polym. Adv. Technol. 29 (2018) 1271–1277. https://doi.org/10.1002/pat.4238.
[52] Q. Meng, W. Li, Y. Zheng, Z. Zhang, Effect of poly(methyl methacrylate) addition on the dielectric and energy storage properties of poly(vinylidene fluoride), J. Appl. Polym. Sci. 116 (2010) 2674–2684. https://doi.org/10.1002/app.31777.
[53] M. MacKey, A. Hiltner, E. Baer, L. Flandin, M.A. Wolak, J.S. Shirk, Enhanced breakdown strength of multilayered films fabricated by forced assembly microlayer coextrusion, J. Phys. D. Appl. Phys. 42 (2009). https://doi.org/10.1088/0022-3727/42/17/175304.
[54] Z. Zhou, M. MacKey, J. Carr, L. Zhu, L. Flandin, E. Baer, Multilayered polycarbonate/poly(vinylidene fluoride-co-hexafluoropropylene) for high energy density capacitors with enhanced lifetime, J. Polym. Sci. Part B Polym. Phys. 50 (2012) 993–1003. https://doi.org/10.1002/polb.23094.
[55] J.K. Tseng, S. Tang, Z. Zhou, M. Mackey, J.M. Carr, R. Mu, L. Flandin, D.E. Schuele, E. Baer, L. Zhu, Interfacial polarization and layer thickness effect on electrical insulation in multilayered polysulfone/poly(vinylidene fluoride) films, Polym. (United Kingdom). 55 (2014) 8–14. https://doi.org/10.1016/j.polymer.2013.11.042.
[56] H. Huang, X. Chen, K. Yin, I. Treufeld, D.E. Schuele, M. Ponting, D. Langhe, E. Baer, L. Zhu, Reduction of Ionic Conduction Loss in Multilayer Dielectric Films by Immobilizing Impurity Ions in High Glass Transition Temperature Polymer Layers, ACS Appl. Energy Mater. 1 (2018) 775–782. https://doi.org/10.1021/acsaem.7b00211.
[57] Y. Wang, J. Cui, Q. Yuan, Y. Niu, Y. Bai, H. Wang, Significantly Enhanced Breakdown Strength and Energy Density in Sandwich-Structured Barium Titanate/Poly(vinylidene fluoride) Nanocomposites, Adv. Mater. 27 (2015) 6658–6663. https://doi.org/10.1002/adma.201503186.
[58] Y. Wang, L. Wang, Q. Yuan, Y. Niu, J. Chen, Q. Wang, H. Wang, Ultrahigh electric displacement and energy density in gradient layer-structured BaTiO3/PVDF nanocomposites with interfacial barrier effect, J. Mater. Chem. A. 5 (2017) 10849–10855. https://doi.org/10.1039/C7TA01522D.
[59] Y. Shen, D. Shen, X. Zhang, J. Jiang, Z. Dan, Y. Song, Y. Lin, M. Li, C.W. Nan, High energy density of polymer nanocomposites at a low electric field induced by modulation of their topological-structure, J. Mater. Chem. A. 4 (2016) 8359–8365. https://doi.org/10.1039/c6ta02186g.
[60] Y. Wang, J. Chen, Y. Li, Y. Niu, Q. Wang, H. Wang, Multilayered hierarchical polymer composites for high energydensity capacitors, J. Mater. Chem. A. 7 (2019) 2965–2980.
[61] L. Wang, H. Luo, X. Zhou, X. Yuan, K. Zhou, D. Zhang, Sandwich-structured all-organic composites with high breakdown strength and high dielectric constant for film capacitor, Compos. Part A Appl. Sci. Manuf. 117 (2019) 369–376. https://doi.org/10.1016/j.compositesa.2018.12.007.
[62] J. Jiang, Z. Shen, J. Qian, Z. Dan, M. Guo, Y. He, Y. Lin, C.W. Nan, L. Chen, Y. Shen, Synergy of micro-/mesoscopic interfaces in multilayered polymer nanocomposites induces ultrahigh energy density for capacitive energy storage, Nano Energy. 62 (2019) 220–229. https://doi.org/10.1016/j.nanoen.2019.05.038.
[63] Y. Wang, Y. Li, L. Wang, Q. Yuan, J. Chen, Y. Niu, X. Xu, Q. Wang, H. Wang, Gradient-layered polymer nanocomposites with significantly improved insulation performance for dielectric energy storage, Energy Storage Mater. 24 (2020) 626–634. https://doi.org/10.1016/j.ensm.2019.06.013.
[64] Y. Zhu, P. Jiang, X. Huang, Enhancing discharged energy density and suppressing dielectric loss of poly (vinylidene chlorofluoroethylene) by a sandwiched structure, 1 (2018) 127–131. https://doi.org/10.1049/iet-nde.2018.0011.
[65] F. Liu, Q. Li, J. Cui, Z. Li, G. Yang, Y. Liu, L. Dong, C. Xiong, H. Wang, Q. Wang, High-Energy-Density Dielectric Polymer Nanocomposites with Trilayered Architecture, Adv. Funct. Mater. 27 (2017) 1–7. https://doi.org/10.1002/adfm.201606292.
[66] J.K. Tseng, K. Yin, Z. Zhang, M. Mackey, E. Baer, L. Zhu, Morphological effects on dielectric properties of poly(vinylidene fluoride-co-hexafluoropropylene) blends and multilayer films, Polymer (Guildf). 172 (2019) 221–230. https://doi.org/10.1016/j.polymer.2019.03.076.
[67] X. Chen, J.-K. Tseng, I. Treufeld, M. Mackey, D. Schuele, R. Li, M. Fukuto, E. Baer, L. Zhu, Enhanced Dielectric Properties from Space Charge-Induced Interfacial Polarization in Multilayer Polymer Films, J. Mater. Chem. C. (2017). https://doi.org/10.1039/C7TC03653A.
[68] L. Yang, J. Ho, E. Allahyarov, R. Mu, L. Zhu, Semicrystalline structure-dielectric property relationship and electrical conduction in a biaxially oriented poly(vinylidene fluoride) film under high electric fields and high temperatures, ACS Appl. Mater. Interfaces. 7 (2015) 19894–19905. https://doi.org/10.1021/acsami.5b02944.
[69] K.C. Kao, 6 - Charge Carrier Injection from Electrical Contacts, in: K.C.B.T.-D.P. in S. Kao (Ed.), Academic Press, San Diego, 2004: pp. 327–380. https://doi.org/https://doi.org/10.1016/B978-012396561-5/50016-5.
[70] M. Roy, J.K. Nelson, R.K. MacCrone, L.S. Schadler, C.W. Reed, R. Keefe, Polymer nanocomposite dielectrics-the role of the interface, IEEE Trans. Dielectr. Electr. Insul. 12 (2005) 629–643. https://doi.org/10.1109/TDEI.2005.1511089.
[71] G. Brinati, A. Marrani, B. Goffaux, Vinylidene fluoride and trifluoroethylene containing polymers, (2011). https://www.google.com/patents/US20110082271.
[72] J. Link, O. Sanseau, M. Tauban, F. Colbeau-Justin, C. Lorthioir, P. Sotta, Thermoreversible Gelation of a Vinylidene Fluoride-Based Copolymer in Methyl Ethyl Ketone: Dynamics and Structure, Macromol. Symp. 385 (2019) 1800162. https://doi.org/10.1002/masy.201800162.
[73] Q. Liu, C. Richard, J.F. Capsal, Control of crystal morphology and its effect on electromechanical performances of electrostrictive P(VDF-TrFE-CTFE) terpolymer, Eur. Polym. J. 91 (2017) 46–60. https://doi.org/10.1016/j.eurpolymj.2017.03.046.
[74] X. Zhou, X. Zhao, Z. Suo, C. Zou, J. Runt, S. Liu, S. Zhang, Q.M. Zhang, Electrical breakdown and ultrahigh electrical energy density in poly(vinylidene fluoride-hexafluoropropylene) copolymer, Appl. Phys. Lett. 94 (2009) 5–7. https://doi.org/10.1063/1.3123001.

[75] K.C. Kao, 7 - Electrical Conduction and Photoconduction, in: K.C. Kao (Ed.), Dielectr. Phenom. Solids, Academic Press, San Diego, 2004: pp. 381–514. https://doi.org/https://doi.org/10.1016/B978-012396561-5/50017-7.
[76] J.F. Capsal, M. Lallart, J. Galineau, P.J. Cottinet, G. Sebald, D. Guyomar, Evaluation of macroscopic polarization and actuation abilities of electrostrictive dipolar polymers using the microscopic Debye/Langevin formalism, J. Phys. D. Appl. Phys. 45 (2012). https://doi.org/10.1088/0022-3727/45/20/205401.
[77] M. Lallart, J.F. Capsal, G. Sebald, P.J. Cottinet, D. Guyomar, Converse electrostrictive effect in dielectric polymers, Sensors Actuators, B Chem. 190 (2014) 259–264. https://doi.org/10.1016/j.snb.2013.08.028.
[78] X. Hao, A review on the dielectric materials for high energy-storage application, J. Adv. Dielectr. 03 (2013) 1330001. https://doi.org/10.1142/s2010135x13300016.
[79] Z. Yao, Z. Song, H. Hao, Z. Yu, M. Cao, S. Zhang, M.T. Lanagan, H. Liu, Homogeneous/Inhomogeneous-Structured Dielectrics and their Energy-Storage Performances, Adv. Mater. 29 (2017). https://doi.org/10.1002/adma.201601727.
[80] Q. Liu, Development of electrostrictive P(VDF-TrFE-CTFE) terpolymer for inkjet printed electromechanical devices, INSA Lyon, 2016.
[81] A.A. Zabolotskii, Local Electric Fields in Ensembles of Composite Nanoparticles, 52 (2016) 388–395.
[82] Z. Cai, X. Wang, B. Luo, W. Hong, L. Wu, L. Li, Dielectric response and breakdown behavior of polymer-ceramic nanocomposites: The effect of nanoparticle distribution, Compos. Sci. Technol. 145 (2017) 105–113. https://doi.org/10.1016/j.compscitech.2017.03.039.
[83] H.M. Bao, J.F. Song, J. Zhang, Q.D. Shen, C.Z. Yang, Q.M. Zhang, Phase transitions and ferroelectric relaxor behavior in P(VDF-TrFE-CFE) terpolymers, Macromolecules. 40 (2007) 2371–2379. https://doi.org/10.1021/ma062800l.
[84] F. Bargain, T. Soulestin, F. Domingues Dos Santos, V. Ladmiral, B. Améduri, S. Tencé-Girault, Semicrystalline Organization of VDF- and TrFE-Based Electroactive Terpolymers: Impact of the trans-1,3,3,3-Tetrafluoropropene Termonomer, Macromolecules. 50 (2017) 3313–3322. https://doi.org/10.1021/acs.macromol.7b00051.
[85] M. Sharma, G. Madras, S. Bose, Cooperativity and Structural Relaxations in PVDF/PMMA Blends in the Presence of MWNTs: An Assessment through SAXS and Dielectric Spectroscopy, Macromolecules. 47 (2014) 1392–1402. https://doi.org/10.1021/ma4023718.
[86] J.F. Capsal, E. Dantras, C. Lacabanne, Molecular mobility interpretation of the dielectric relaxor behavior in fluorinated copolymers and terpolymers, J. Non. Cryst. Solids. 363 (2013) 20–25. https://doi.org/10.1016/j.jnoncrysol.2012.12.008.
[87] X. Yin, Q. Liu, J. Galineau, P.J. Cottinet, D. Guyomar, J.F. Capsal, Enhanced electromechanical performances in plasticizer modified electrostrictive polymers, Eur. Polym. J. 76 (2016) 88–98. https://doi.org/10.1016/j.eurpolymj.2016.01.030.
[88] Z. Zhou, J. Carr, M. Mackey, K. Yin, D. Schuele, L. Zhu, E. Baer, Interphase/interface modification on the dielectric properties of polycarbonate/poly(vinylidene fluoride-co-hexafluoropropylene) multilayer films for high-energy density capacitors, J. Polym. Sci. Part B Polym. Phys. 51 (2013) 978–991. https://doi.org/10.1002/polb.23296.
[89] L. Zhao, G.Z. Liu, J.C. Su, Y.F. Pan, X.B. Zhang, Investigation of thickness effect on electric breakdown strength of polymers under nanosecond pulses, IEEE Trans. Plasma Sci. 39 (2011) 1613–1618. https://doi.org/10.1109/TPS.2011.2143435.
[90] G. Chen, J. Zhao, S. Li, L. Zhong, Origin of thickness dependent dc electrical breakdown in dielectrics, Appl. Phys. Lett. 100 (2012). https://doi.org/10.1063/1.4721809.
[91] B. Helgee, P. Bjellheim, Electric Breakdown Strength of Aromatic Polymers: Dependence on Film Thickness and Chemical Structure, IEEE Trans. Electr. Insul. 26 (1991) 1147–1152. https://doi.org/10.1109/14.108152.
[92] E.Y. Wu, On the Weibull Shape Factor of Intrinsic Breakdown of Dielectric Films and Its Accurate Experimental Determination — Part I : Theory , Methodology , Experimental Techniques, IEEE Trans. Electron Devices. 49 (2002) 2131–2140. https://doi.org/Doi 10.1109/Ted.2002.805612.
[93] Y. Tanaka, N. Ohnuma, K. Katsunami, Y. Ohki, Effects of Crystallinity and Electron Mean-free-path on Dielectric Strength of Low-density Polyethylene, IEEE Trans. Electr. Insul. 26 (1991) 258–265. https://doi.org/10.1109/14.78326.
[94] I. Rytöluoto, A. Gitsas, S. Pasanen, K. Lahti, Effect of film structure and morphology on the dielectric breakdown characteristics of cast and biaxially oriented polypropylene films, Eur. Polym. J. 95 (2017) 606–624. https://doi.org/10.1016/j.eurpolymj.2017.08.051.
[95] P. Hu, Y. Shen, Y. Guan, X. Zhang, Y. Lin, Q. Zhang, C.W. Nan, Topological-structure modulated polymer nanocomposites exhibiting highly enhanced dielectric strength and energy density, Adv. Funct. Mater. 24 (2014) 3172–3178. https://doi.org/10.1002/adfm.201303684.

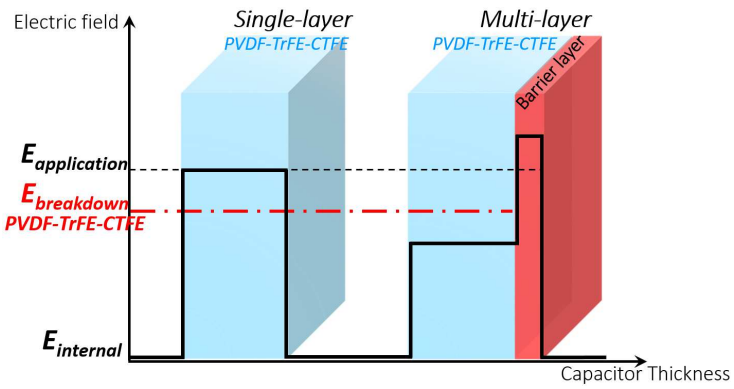
Electric field
Single-layer
PVDF-TrFE-CTFE
Multi-layer
PVDF-TrFE-CTFE
Barrier layer
E application
E breakdown
PVDF-TrFE-CTFE
E internal
Capacitor Thickness